Title

Networks of energetic and metabolic interactions define dynamics in microbial communities

Journal

Proceedings of the National Academy of Sciences of the United States of America, 112(50)

ISSN

0027-8424

Authors

Embree, Mallory
Liu, Joanne K
Al-Bassam, Mahmoud M
et al.

Publication Date

2015-12-15

DOI

10.1073/pnas.1506034112

Peer reviewed

Networks of energetic and metabolic interactions define dynamics in microbial communities

Mallory Embree, Joanne K. Liu, Mahmoud M. Al-Bassam, and Karsten Zengler[1]

Department of Bioengineering, University of California, San Diego, CA 92091

Edited by Mary E. Lidstrom, University of Washington, Seattle, WA, and approved October 21, 2015 (received for review March 26, 2015)

Microorganisms form diverse communities that have a profound impact on the environment and human health. Recent technological advances have enabled elucidation of community diversity at high resolution. Investigation of microbial communities has revealed that they often contain multiple members with complementing and seemingly redundant metabolic capabilities. An understanding of the communal impacts of redundant metabolic capabilities is currently lacking; specifically, it is not known whether metabolic redundancy will foster competition or motivate cooperation. By investigating methanogenic populations, we identified the multidimensional interspecies interactions that define composition and dynamics within syntrophic communities that play a key role in the global carbon cycle. Species-specific genomes were extracted from metagenomic data using differential coverage binning. We used metabolic modeling leveraging metatranscriptomic information to reveal and quantify a complex intertwined system of syntrophic relationships. Our results show that amino acid auxotrophies create additional interdependencies that define community composition and control carbon and energy flux through the system while simultaneously contributing to overall community robustness. Strategic use of antimicrobials further reinforces this intricate interspecies network. Collectively, our study reveals the multidimensional interactions in syntrophic communities that promote high species richness and bolster community stability during environmental perturbations.

microbial communities | microbiome | interspecies interactions | methanogens | metabolic modeling

Microorganisms coexisting in nature engage in a variety of interactions, resulting in collaboration and competition between individual community members. Advances in microbial ecology have revealed high levels of species diversity and complexity in most communities (1–3). Although we can readily determine the community composition, we currently lack a deeper understanding of how these communities are assembled and how diversity is maintained. Obligately syntrophic communities, the potential origin of the eukaryotic cell (4), consist of microorganisms with metabolisms that are thermodynamically linked and catabolically interdependent. These communities are essential for the global carbon cycle by decomposing organic matter to CO_2 and methane.

The close interactions between anaerobic bacteria and archaea enable degradation of carbohydrates, proteins, and lipids but also, recalcitrant matter, such as alkanes. Syntrophic oxidation of alkanes can occur in communities consisting of three interacting species (5, 6), whereas degradation of simple fatty acids, such as caprylate, has been shown with three microorganisms, and butyrate has been shown with two microorganisms. Here, we show that five members govern hexadecane degradation in a community (Fig. 1 *A–D*) that has been maintained in the laboratory for over 15 y and serially passaged more than 40 times (6, 7). However, when transferred to fatty acid-containing media (Fig. 1 *B* and *C*), four- and three-member communities dominate caprylate and butyrate degradation, respectively (6, 7). Because syntrophic communities operate near thermodynamic equilibrium, the presence of additional organisms within the communities prompted the investigation of interspecies interactions and dependencies within these microbial communities to identify the underlying factors that influence community composition. Several metabolic redundancies exist between the individual species within these communities, but bacteria and archaea all seem to collectively persist and thrive. The layering of multiple types of interspecies interactions, particularly those that extend beyond basic carbon exchange, may explain the presence of seemingly redundant species diversity within this community. Amino acid auxotrophy has been shown to increase the stability of a synthetic community of *Escherichia coli* strains (8). Studying the interspecies interactions and dependencies within natural microbial communities is necessary to determine the factors that define community composition. Here, we describe how multilevel interactions that extend beyond catabolic requirements define microbial diversity and dynamics in methanogenic communities (6, 7).

Results

Revealing Community Structure. DNA and RNA were harvested from the three communities (Fig. 1 *A–C*) for metagenomic and metatranscriptomic sequencing. The hexadecane-degrading community served as initial inoculum for cultures that were established to oxidize caprylic or butyric acid syntrophically. Despite numerous (over 40) serial passages into hexadecane-containing medium over the course of 15 y, dormant members undetectable by 16S rDNA sequencing became dominant when provided with fatty acids within 4 mo of passing (Fig. 1*E*). Metagenomic datasets acquired from the three different communities were used for differential coverage metagenomic binning (9). In total, seven nearly complete genomes representing the seven most dominant organisms (Fig. 1*E*) were obtained and annotated (10) (Table 1, Fig. S1, and Dataset S1). Compared with sequenced relatives, the genomes exhibited the highest

Significance

Microbial communities are critical to global carbon cycling and particularly important in oxygen-limited environments, such as sediments and parts of the human microbiome. However, the uncultured members of these communities often hinder the study of community composition and interspecies interactions at a deeper level. Here, we integrate metagenomic binning, metatranscriptomic analysis, and metabolic modeling to obtain quantitative information about interspecies interactions between individual species present in methanogenic communities. We found that these communities are defined by not only metabolic interactions but also additional interdependencies, such as amino acid auxotrophies. Strategic usage of antimicrobials by specific community members further reinforces this intricate interspecies network, thereby enforcing strong collaboration among community members.

Author contributions: M.E. and K.Z. designed research; M.E., M.M.A.-B., and K.Z. performed research; M.E., J.K.L., and K.Z. analyzed data; and M.E., J.K.L., and K.Z. wrote the paper.

The authors declare no conflict of interest.

This article is a PNAS Direct Submission.

Data deposition: The transcriptomics data reported in this paper have been deposited in the Gene Expression Omnibus (GEO) database, www.ncbi.nlm.nih.gov/geo (accession no. GSE498301). This Whole Genome Shotgun project has been deposited at DDBJ/EMBL/GenBank under the accession no. LNQE00000000.

[1]To whom correspondence should be addressed. Email: kzengler@ucsd.edu.

This article contains supporting information online at www.pnas.org/lookup/suppl/doi:10.1073/pnas.1506034112/-/DCSupplemental.

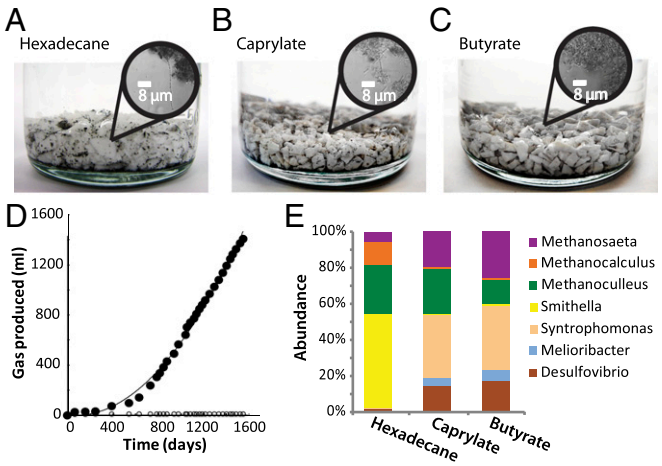

Fig. 1. Growth of methanogenic communities. (*A*) Teflon boiling stones were coated with hexadecane to increase the contact between cells and the hydrophobic substrate. The methanogenic community propagated in 300 mL mineral medium (6) containing 20 mM hexadecane grows very slowly to low biomass density. The hexadecane community was passed onto medium containing (*B*) 2 mM caprylate or (*C*) 5 mM butyrate. All communities grew to very low biomass densities, despite being very metabolically active as indicated by gas (methane) bubbles formed. (*D*) The methanogenic community formed a total of 1,407 mL methane after 1,551 d of incubation (black circles). The control containing no substrate (white circles) did not form any methane. Growth curves of the fatty acid cultures were previously published (7). (*E*) Metagenomic sequencing reads were mapped back to the newly acquired genomes to establish species abundance in the community under hexadecane-, caprylate-, and butyrate-degrading conditions. Numbers of mapped reads were normalized by genome size.

levels of similarity to *Smithella* sp. ME-1, *Syntrophomonas wolfei*, *Desulfovibrio magneticus*, *Methanoculleus marisnigri*, *Methanosaeta concilii*, *Methanocorpusculum labreanum*, and *Melioribacter roseus* (Fig. S1). The community propagated on hexadecane was the source for the *Smithella* sp. ME-1 genome obtained previously by a single-cell approach (7), and therefore, the high sequence similarity between the binned *Smithella* genome and *Smithell*a sp. ME-1 was expected.

Transcriptomic datasets were mapped to these genomes to obtain species-specific gene expression profiles of community members under each condition. These genomes also served as the basis for genome-scale metabolic reconstructions that were used to simulate and quantify interspecies interactions.

Quantifying Interspecies Interactions. Growth with hexadecane resulted in five metabolically active community members: two hydrogenotrophic methanogens *Methanocalculus* and *Methanoculleus*, acetoclastic *Methanosaeta*, alkane-activating *Smithella*, and sulfate-reducing *Desulfovibrio* (Fig. 2*A*). The complexity and overlap in metabolic capability inherent to this community hindered the ability to elucidate all interactions by genomic and transcriptomic analysis alone. Furthermore, because sulfate is not being reduced in this community, *Desulfovibrio*'s role in the hexadecane-degrading community was unclear. Thus, we quantified interactions between species using individual genome-scale metabolic models. Unlike kinetic models, which leverage thermodynamics and chemical concentrations to describe systems, metabolic models are networks of metabolic pathways that link the genome with physiology. Initial draft models for *Smithella* and *Desulfovibrio* were generated using ModelSEED (11), whereas the methanogen models were built off of an existing model of *Methanosarcina barkeri* (12). All models were curated (Dataset S2) using genome and physiological information. The *Smithella* model, in particular, required the addition of a hexadecane-degrading pathway as well as a functional β-oxidation pathway. Although the exact hexadecane activation method in *Smithella* is unknown and cannot be reconciled easily, these models are phenomenological, suggesting that, even if a molecular mechanism is not completely understood, it can be represented in the model if we understand the basic stoichiometry.

Simulations with the model were based off of experimentally measured hexadecane uptake and methane production rates (Fig. 1*D*). Because of the slow-growing, low-biomass nature of the community, hexadecane uptake and methane evolution were used as the objective functions for *Smithella* and the methanogens, respectively, instead of biomass. Because *Smithella* is the hexadecane degrader of this community, the hexadecane uptake rate was used in the *Smithella* model to calculate the amount of syntrophic intermediates generated per 1 mmol hexadecane. Similarly, the methane production rate was divided among the methanogens based on abundance, because rates of methanogenesis have been shown to be very closely related to growth rate (13). These production rates were then used to backcalculate the syntrophic intermediate needs of each methanogen in the community. These values were then analyzed and compared with identified discrepancies in energy flow within the system to identify potential metabolic roles for *Desulfovibrio*. Integration of transcriptomic data with these models was used to further highlight active subsystems and pathways (Dataset S3).

Our modeling results predict that *Smithella* generates hydrogen, formate, and acetate during hexadecane degradation (Fig. 2*B*). The majority of 10 mmol formate is being consumed by *Methanocalculus*. However, the models suggest that *Smithella* only produces 9.4 mmol hydrogen per 1 mmol hexadecane, which would be insufficient for 14.56 mmol hydrogen, which *Methanoculleus* needs to produce the observed amount of methane. We hypothesize that *Desulfovibrio* may remedy this shortage by converting excess formate into hydrogen by formate hydrogen lyase (Dataset S2). Cocultures of *Desulfovibrio* and *Methanobrevibacter* have been reported to couple this reaction to energy conservation at low hydrogen partial pressures (14). *Desulfovibrio* may use this mechanism under hexadecane-degrading conditions for energy conservation, thus creating a second layer of syntrophy within the community (Fig. 2*B*).

Although species abundance analysis suggests similar community composition during caprylate and butyrate degradation (Fig. 1*E*), transcriptomic profiles suggest distinct activity for each species under each condition (Dataset S3). *Syntrophomonas* serves as the primary butyrate metabolizer, with *Desulfovibrio* and *Methanoculleus* as its syntrophic partners (Fig. 2*A*). Butyrate degradation creates hydrogen/formate and acetate (Table 2) (15). The hydrogenotrophic *Methanoculleus* uses hydrogen. *Desulfovibrio* can also metabolize hydrogen when coupled to sulfate reduction, making it a potential competitor against *Methanoculleus*. Sulfate reducers will typically outcompete methanogens for hydrogen in the presence of sulfate (16). However, no sulfate reduction could be measured in this community. Instead, *Desulfovibrio* may again be using formate to generate additional hydrogen for *Methanoculleus* by formate hydrogen lyase. Because no acetoclastic methanogens are active (based on read mapping and quantitative PCR), *Desulfovibrio* is likely assimilating acetate and CO_2 for anabolism (17). In the caprylate community, *Syntrophomonas* uses caprylate and produces hydrogen/formate for *Methanoculleus* and *Desulfovibrio*. Additional acetate generated during caprylate degradation (Table 2) likely allows the acetoclastic *Methanosaeta* to become active and coexist with *Desulfovibrio*.

Table 1. Genomes obtained by differential coverage binning

Organism	Genome size (Mb)	Contigs/genes
Desulfovibrio	3.32	364/3,045
Melioribacter	2.80	469/2,385
Smithella	3.23	229/3,284
Syntrophomonas	3.17	114/3,184
Methanosaeta	2.77	171/3,008
Methanocalculus	2.13	288/2,554
Methanoculleus	2.32	289/2,552

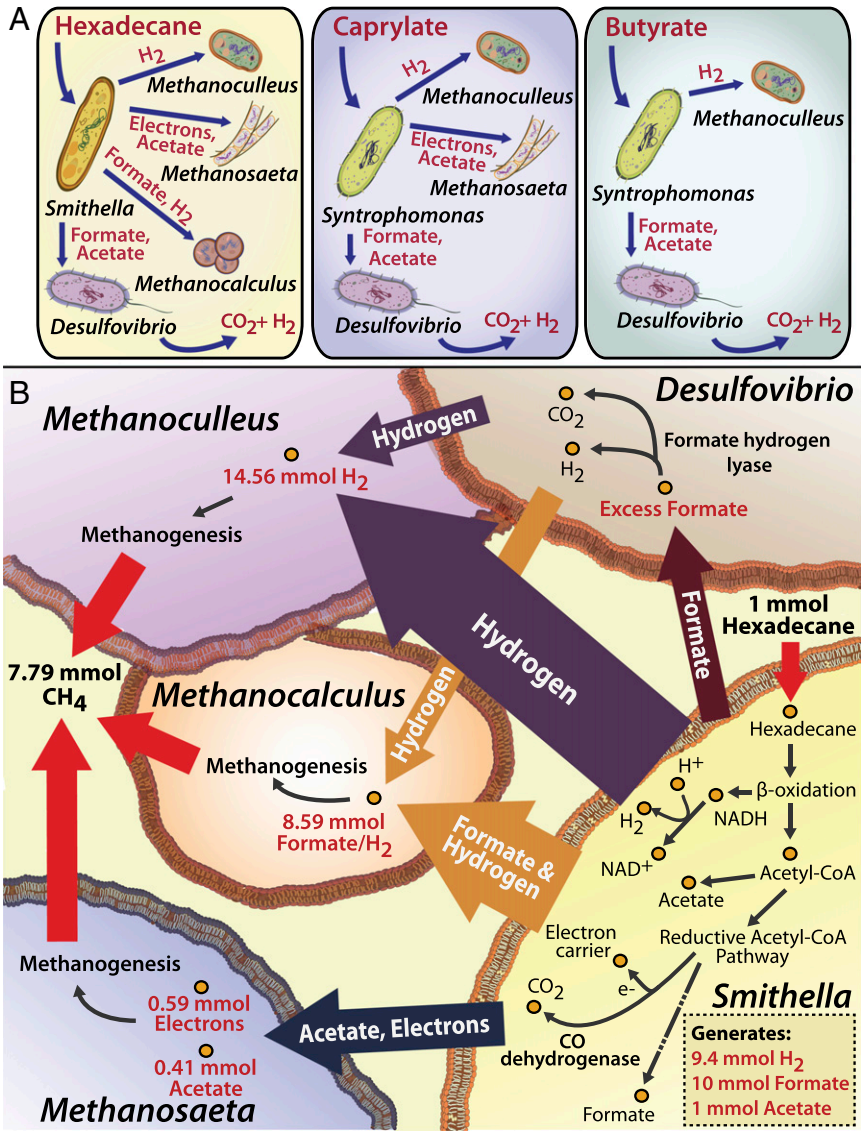

Fig. 2. Complex interspecies interactions driving syntrophy. (*A*) Metabolic interspecies interactions in three communities as determined by transcriptomic information. (*B*) Interspecies exchanges as calculated by metabolic modeling using physiological data for the hexadecane uptake and methane production rates. Flux values are being reported as absolute values (extrapolated over the time represented by the physiological measurements) rather than rate. Hexadecane initially degraded by *Smithella* results in reducing equivalents that are passed to its syntrophic partners *Methanoculleus*, *Methanocalculus*, *Methanosaeta*, and *Desulfovibrio* in various forms. *Desulfovibrio* is converting formate to hydrogen and CO_2, possibly forming its own syntrophic interactions with the methanogens.

Amino Acid Auxotrophy Heightens Dependence. Our analysis shows that a complex, intertwined catabolic network exists between the different species in these three communities. Energy-rich substrates (Table 2) enabled more complex interactions to achieve optimal transfer of reducing power (18), thus leading to greater metabolic and species diversity. However, the benefit for these communities operating near thermodynamic equilibrium to support multiple, coexisting community members with seemingly similar metabolic niches was unclear. Thus, we investigated alternate factors that could influence community composition and robustness. Strikingly, we found that no single species in these communities is capable of synthesizing an entire suite of amino acids, implying that amino acid auxotrophies also govern interspecies interactions in syntrophic communities (Fig. 3*A*). Ranking of the amino acids according to their cost of biosynthesis, with tryptophan being the most expensive (8), revealed that the burden of amino acid biosynthesis is not distributed evenly among all community members (Fig. 3*B*). Previous studies have shown that amino acid exchange may complement hydrogen transfer as an interspecies electron carrier in synthetic, syntrophic cocultures (19), prompting us to further investigate amino acid transfer in this community.

In addition to providing the most biosynthetically expensive amino acids, *Smithella* and *Syntrophomonas* are the sole providers of histidine and tyrosine in their respective communities. *Desulfovibrio* fortifies its position within the community by being the only community member capable of methionine biosynthesis under caprylate and butyrate conditions. It is also the exclusive provider of proline during hexadecane degradation. Thus, dominating an important niche of amino acid synthesis elevates *Desulfovibrio* into a valuable syntrophic partner, despite its thermodynamic disadvantage over methanogens (15). Methanogens are significantly more auxotrophic for amino

Table 2. Gibbs free energy of key reactions involved in syntrophic degradation of hexadecane, caprylate, and butyrate

Reaction	ΔG
$4H_2 + HCO_3^- + H^+ \rightarrow CH_4 + 3H_2O$	−99 kJ/rxn
$Formate^- + H_2O \rightarrow H_2 + HCO_3^-$	−35 kJ/rxn
$Acetate + H_2O \rightarrow HCO_3^- + CH_4$	−67 kJ/rxn
$Butyrate + 2H_2O \rightarrow 2Acetate + H^+ + 2H_2$	−48 kJ/rxn
$Caprylate + 6H_2O \rightarrow 4Acetate + 3H^+ + 6H_2$	−145 kJ/rxn
$Hexadecane + 16H_2O \rightarrow 8Acetate + 8H^+ + 17H_2$	−486 kJ/rxn
$2Butyrate + 5H_2O \rightarrow 3HCO_3^- + H^+ + 5CH_4$	−136 kJ/mol
$2Caprylate + 11H_2O \rightarrow 5HCO_3^- + 3H^+ + 11CH_4$	−273 kJ/mol
$4Hexadecane + 45H_2O \rightarrow 15HCO_3^- + 15H^+ + 49CH_4$	−492 kJ/mol

rxn, reaction.

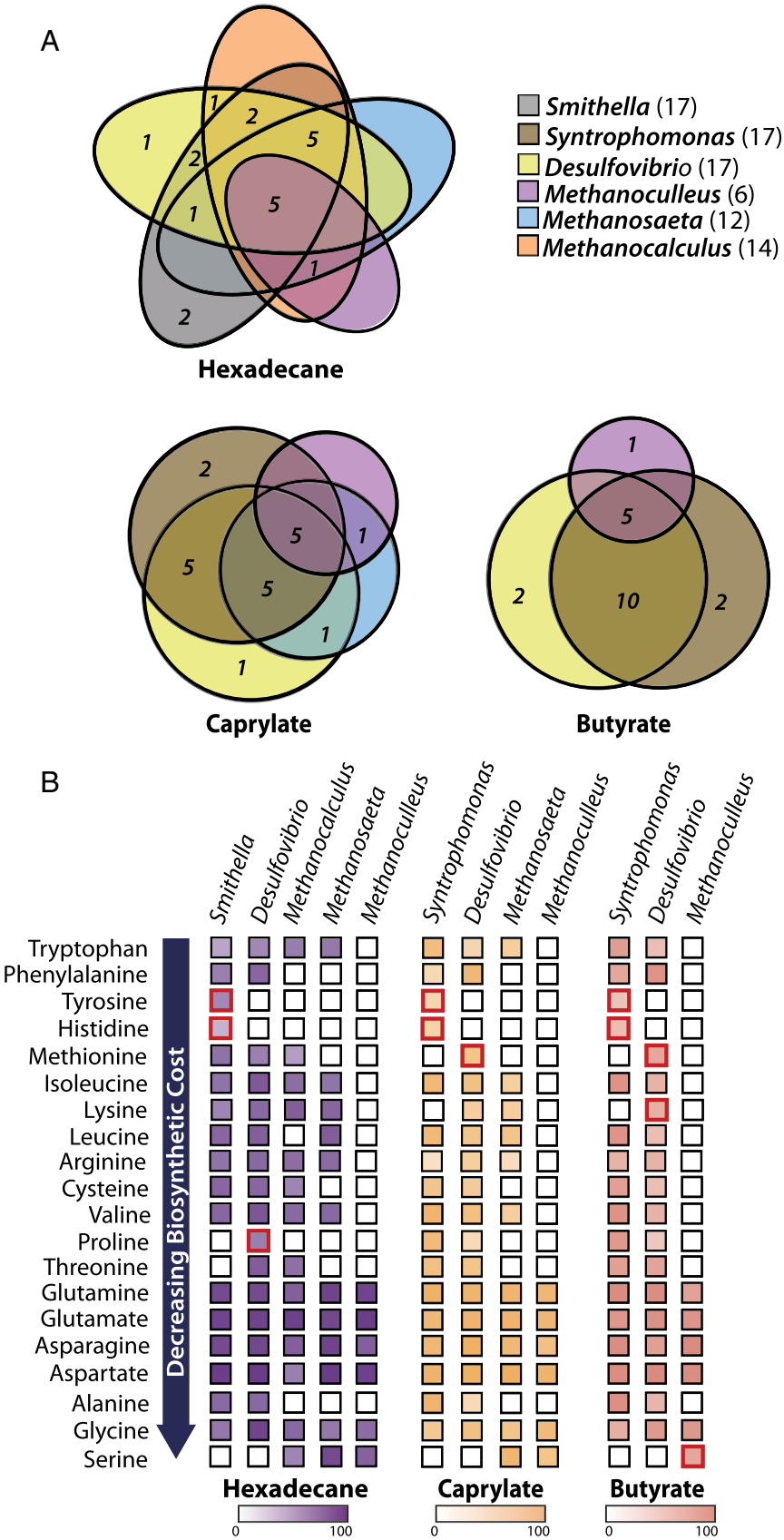

Fig. 3. Amino acid auxotrophies shape community composition. (*A*) Overlap of amino acid biosynthesis capabilities between community members in communities growing with hexadecane, caprylate, or butyrate. Numbers in parentheses refer to the numbers of amino acids that the particular species can produce. (*B*) Specific amino acid auxotrophies present in each species for each community. Amino acids have been ranked according to biosynthetic cost (arrow) (8). A colored square denotes that a species can synthesize an amino acid. The intensity of each color (based on the scale) represents the relative expression of the synthesis pathways (*Methods*), with darker/more intense color indicating higher expression. Amino acids exclusively produced by one microorganism are highlighted in red.

acids than bacteria but the sole providers of serine in all three communities. Although serine is relatively inexpensive to synthesize, all methanogens have an additional ability to generate serine during methanogenesis by serine hydroxymethyltransferase (Dataset S1).

During growth with butyrate, we found that five amino acids are synthesized by only one of three community members (Fig. 3*B*). However, when grown on caprylate, the community includes *Methanosaeta* as the fourth active member. *Methanosaeta*'s growth is caused by the presence of additional acetate, but interestingly, it also synthesizes two (lysine and serine) of five exclusive amino acids in the butyrate community. This redundancy reduces essential dependencies between species and spreads amino acid biosynthetic burden.

The *Smithella* genome encodes an active MazEF toxin-antitoxin system. MazEF induces autolysis in response to low concentrations of external amino acids. To test if autolysis is a potential source of amino acids, liquid chromatography (LC) -MS was used to analyze the culture media for evidence of amino acids. Trace amino acids were undetectable in the media, suggesting that amino acids are not provided through cell lysis alone. Because free amino acids were undetectable by LC-MS/MS (detection limit 0.001–1 μM), we confirmed active amino acid biosynthesis by transcriptomics. *Smithella* and *Syntrophomonas* generally have higher average pathway expression values (~30% higher) than other community members capable of synthesizing the same amino acid (Fig. 3*B*). This activity is most apparent during growth with butyrate. Although *Syntrophomonas* and *Desulfovibrio* have similar capabilities for synthesizing amino acids, *Syntrophomonas* exhibits higher average expression levels for eight of the biosynthesis pathways, whereas *Desulfovibrio* only has higher expression for phenylalanine, suggesting that the primary metabolizers take the majority of the biosynthetic burden. Amino acid biosynthesis is an energy-intensive process, and therefore, supplementation by the bacteria may enable the methanogens to focus their metabolism on methanogenesis and the uptake of reducing equivalents rather than biosynthesis. The luxury of amino acid supplementation would ease the energetic burden on the methanogens, which in turn, would allow them to maintain the appropriate thermodynamic requirements for syntrophy with *Smithella* and *Syntrophomonas*.

Colicin V Solidifies the Syntrophic Unit. Although amino acid auxotrophies reinforce interdependence and collaboration within these communities, they are vulnerable to invading, competing species. We found that *Desulfovibrio* encodes a full set of genes for synthesis of colicin V. This type of bacteriocin enters the cell using a Ton or Tol system, killing cells through membrane depolarization by pore formation (20). Colicin V may be used as a defensive mechanism in these communities. Resistance to colicin V coalesces as a series of mutations that inactivate bacteriocin uptake. The *Syntrophomonas*, *Methanoculleus*, *Methanosaeta*, and *Methanocalculus* genomes do not encode any functional Ton or Tol system, rendering these species immune to colicin V. Immunity to colicin V may have allowed *Syntrophomonas* to outcompete *Smithella* during caprylate and butyrate degradation. Similarly, *Melioribacter*'s presence but apparent metabolic inactivity across all conditions may be a consequence of a colicin V exposure, because its genome encodes nine genes related to Tol and Ton systems (Dataset S1). Additional investigations will be required to determine colicin V's impact on community structure.

Discussion

Although recent technologies have enabled the study of individual species within natural microbial communities at a resolution previously limited to axenic cultures (6, 7), we have been unable to decipher all underlying factors that define community composition and dynamics. The community systems biology approach (21) deployed here delineated the multidimensional interactions that shape and maintain microbial communities. Species with similar metabolic capabilities are collaborating in favor of maximizing dissemination energy through the community in the form of electrons and electron carriers (18). As substrates became more energy-rich, the syntrophic community shifted and diversified its composition to better accommodate the transfer of reducing equivalents. The butyrate-degrading community had three active members, the caprylate-degrading community had four active members, and the community cultured on hexadecane, the most energy-rich substrate, involved five active species. The expansion of the active community increased the mechanisms for transfer of reducing equivalents used by the key members, allowing the entire community to benefit. Although reducing equivalent transfer is a defining characteristic of a syntrophic interaction, we found that the factors that influence community composition extend beyond catabolism to include amino acid exchanges and potentially, bacteriocin use. Cumulatively, these interactions and dependencies create stability within the community by allowing for the preservation of metabolic redundancy among community members. Although previous studies have suggested that competition and commensalism drive community assembly (22), cooperation and mutualism may ultimately account for maintenance of species heterogeneity in methanogenic communities essential for the global carbon cycle but moreover, help us understand community diversity and evolution in different environments.

The combination of systems and molecular biology will allow additional investigation into the specifics of species' interactions. Metabolic models enable us to both hypothesize and analyze the effects of perturbations, such as the addition to free amino acids or the introduction of another organism that supplies essential metabolites. Similarly, we can predict metabolically the types of organisms that may increase diversity levels or simulate possible subpopulations that may evolve maintaining stable interactions. Knowledge of these multidimensional interspecies relationships will be crucial to our ability to predict and exploit the foundational roles that microbial communities play in the environment, for industrial applications, and for human health.

Methods

Media and Cultivation. The source of the original community was sediment from a hydrocarbon-contaminated ditch in Bremen, Germany (6). The consortium was propagated in the laboratory in an anoxic medium containing 0.3 g NH_4Cl, 0.5 g $MgSO_4 \bullet 7H_2O$, 2.5 g $NaHCO_3$, 0.5 g K_2HPO_4, 0.05 g KBr, 0.02 g H_3BO_3, 0.02 g KI, 0.003 g $Na_2WO_2 \bullet 2H_2O$, 0.002 g $NiCl_2 \bullet 6H_2O$, trace elements, and trace minerals as previously described (6). The medium was sparged with a mixture of N_2:CO_2 (80:20, vol/vol), and the pH was adjusted to 7.0. After autoclaving, anoxic $CaCl_2$ (final concentration 0.25 g L^{-1}) and filter-sterilized vitamin solution were added (6). Cells were supplemented with anoxic hexadecane (0.5 mL equaling 1.7 mmol on Teflon stones), 5 mM butyrate, or 2 mM caprylate and incubated at 30 °C in triplicate. Bottles were degassed as necessary to relieve overpressure. The headspace of a representative active culture was analyzed using GC (Shimadzu GC 2014; Supelco 30-m × 0.53-mm Carboxen Column). A thermal conductivity detector was used to identify and quantify the production of methane accompanying cell growth. Ultrapure N_2 was used as carrier gas, and the column was run at 35 °C for 15 min with a flow rate of 20 mL min^{-1}. Hexadecane was analyzed by a gas chromatograph (Shimadzu GC 2014; SHRXI-5ms 15-m × 0.53-mm fused silica column) equipped with a flame ionization detector. The flow rate of H_2 was 1.7 mL min^{-1}. The temperature program was run from 60 °C (2 min isotherm) to 120 °C at 5 °C·min^{-1} and then, from 120 °C (0.1 min isotherm) to 220 °C at 10 °C·min^{-1} (5 min isotherm at 220 °C). The temperatures at the injection port and the detector were 280 °C.

Metagenomic Sequencing. DNA was harvested from the communities during hexadecane-, caprylate-, and butyrate-degrading conditions using a modified version of the Nucleospin XS Tissue Kit. Briefly, 15 mL culture was pelleted by centrifugation at 10,000 × *g* at 4 °C for 10 min. After the initial pelleting, the supernatant was removed and centrifuged again in 1.5-mL microcentrifuge tubes at 14,000 × *g* at 4 °C for an additional 20 min. After centrifugation, the supernatant was decanted, and cell pellets were frozen at −80 °C until use.

Cell pellets were combined and resuspended in 50 μL Tris/EDTA (TE) buffer (10 mM Tris·HCl, 1 mM EDTA, pH 8) with 23,000 U Ready-Lyse Lysozyme Solution (Epicentre), 1 μL Proteinase K Solution (20 mg/mL; Life Technologies), and 1 μL RNase A (100 mg/mL; Qiagen) and incubated at 37 °C for 15 min. After incubation, 50 μL Buffer B3 was added to the sample and vigorously vortexed; 50 μL 100% (vol/vol) ethanol was added to the lysate, and the sample was loaded onto the NucleoSpin Tissue XS Column. From this point, the standard purification protocol was followed.

Sequencing libraries were prepared using the Nextera XT Kit (Illumina). Library quality was assessed using a Bioanalyzer High Sensitivity Chip (Agilent) and quantified using the Qubit dsDNA HS Assay. Standard published protocols were used for both assays. Libraries were sequenced on an Illumina Miseq using 500-cycle kits (Illumina). The metagenome for the hexadecane-degrading community had 10.58 million reads, the caprylate-degrading community had 22.06 million reads, and the butyrate-degrading community had 12.63 million reads.

Metagenomic Binning and Genome Annotation. The reads for each condition were quality trimmed, pooled, and assembled using Velvet (23) to create a pan metagenome. Multiple kmers between 51 and 231 were tested to determine the best kmer length for de novo assembly—the final genome assembly used a kmer of 211. Individual reads were then mapped back to the pan metagenome reference, and the resulting bam files were used as input into GroopM (9). GroopM was run using the default parameters. The preliminary binned genomes were annotated using RAST (10) to determine if any bins needed to be merged—we did not end up merging any bins. We used RAST to check sequence similarity and identify each bin's closest sequenced relative. These results were then matched to species appearing in previously determined 16S rDNA data (7).

The binned genomes' closest relatives were determined using BLASTing the 16S rRNA gene in each metagenomic bin as well as through the Nearest Neighbor function in RAST. The heat maps of sequence similarity were also generated in RAST using the sequence comparison tool.

The amino acid synthesis pathways were curated by hand to ensure accuracy. Resources including KEGG and Metacyc were used as well as primary literature.

Metatranscriptomic Sequencing and Analysis. Metatranscriptomic reads were previously sequenced and published and can be accessed through Gene Expression Omnibus accession no. GSE498301. However, because we did not have accurate reference genomes for all species within the community, we were previously unable to interpret gene expression results for most species within the community (7, 24). Here, we used genomes extracted by GroopM as reference genomes. Reads were mapped as previously described using DESeq (7, 24). The results of the transcriptomic mapping can be found in Dataset S3. When determining whether individual species were active, we used both the number of transcriptomic reads mapped and gffs created from the mapped data. The gffs, in particular, were useful to identify highly transcriptionally active species.

When comparing expression values across species, particularly for amino acid synthesis, genes were first ranked in expression from high to low and assigned percentile values based on the total number of genes in the genome. The percentile values were then compared across species to estimate relative gene expression.

Transcriptomic datasets were also used to help curate amino acid synthesis pathways. In the event that one gene in the pathway was missing, we used the metatranscriptomic datasets to investigate expression levels of the overall pathway. If the overall expression was similar to (or higher than) the species that are capable of synthesizing the amino acid, we considered the species likely to be able to synthesize the amino acid as well.

Metabolomics. Extracellular amino acid concentrations were measured using LC-MS. One milliliter culture from each condition was passed through a 0.22-μm syringe filter (Millipore) and analyzed as previously described on a Synergi 2.5-μm Hydro-RP 100-Å LC Column (100 mm × 2 mm; Phenomenex) with an UFLC XR HPLC (Shimadzu) (25).

Metabolic Modeling Analysis. COBRApy was used for all model building, curation, and simulation efforts (26). Initial draft models for *Smithella* and *Desulfovibrio* were generated using Model-SEED (11). Both models were heavily curated to better represent the physiological functionality captured by the draft genome, and the majority of gap-filled reactions (particularly transporters) were removed. The *Smithella* model was curated to include major metabolic pathways, including functional β-oxidation and the Wood–Ljungdahl pathway. Both pathways exist and are functional within this organism as indicated by genomic and transcriptomic information. Furthermore, because we do not know the exact mode of alkane activation within this organism, a dummy reaction that converts hexadecane into palmitic acid was added to the model to bypass this limitation. The models for the different methanogens were built off of an existing metabolic model for *M. barkeri* (12). Reactions were deleted from the *M. barkeri* model as appropriate for each methanogen based on the genome content found in the binned genomes. A full list of the reactions in each model can be found in Dataset S2.

Simulations were performed using experimentally determined hexadecane uptake rates and methane production rates. Rates of methanogenesis have been shown to be very closely related to growth rate (13), and therefore, the proportion of methane generated by each methanogen was determined based on its abundance within the community as determined by 16S rRNA analysis (Fig. 1*E*). Our models are not integrated into a single-community model. Instead, we performed simulations on each individual model to identify discrepancies in energy flow within the overall system. First, requirements for hydrogen, acetate, formate, and electrons were backcalculated using the models of the methanogenes constraint by the amount of methane produced (Fig. 1). Second, the *Smithella* model was fixed with the measured hexadecane uptake rate to explore the potential solution space and determine if *Smithella* is capable producing this pattern of reducing equivalents. Because of the slow-growing nature of the community, we set hexadecane transfer as the objective function rather than optimizing flux through the biomass function.

ACKNOWLEDGMENTS. We thank Rohini Patel and Janna Tarasova for technical assistance with growth experiments and Ali Ebrahim and Justin Tan for support with COBRApy. We also thank Douglas McCloskey for MS analysis and Helder Balelo for providing photographs. We thank Jennifer Santini and the University of California, San Diego (UCSD) Neuroscience Core and Light Microscopy Facility, which is supported by the UCSD Neuroscience Microscopy Shared Facility Grant P30 NS047101, for microscopy assistance. This study is based on work supported by US Department of Energy (DOE), Office of Science, Office of Biological & Environmental Research Awards DE-SC0004485 and DE-SC0004917. This research relied heavily on the resources of the National Energy Research Scientific Computing Center, a DOE Office of Science User Facility supported by Office of Science of the US DOE Contract DE-AC02-05CH11231.380.

1. Gans J, Wolinsky M, Dunbar J (2005) Computational improvements reveal great bacterial diversity and high metal toxicity in soil. *Science* 309(5739):1387–1390.
2. Eckburg PB, et al. (2005) Diversity of the human intestinal microbial flora. *Science* 308(5728):1635–1638.
3. Sogin ML, et al. (2006) Microbial diversity in the deep sea and the underexplored "rare biosphere." *Proc Natl Acad Sci USA* 103(32):12115–12120.
4. Martin W, Müller M (1998) The hydrogen hypothesis for the first eukaryote. *Nature* 392(6671):37–41.
5. Dolfing J, Larter SR, Head IM (2008) Thermodynamic constraints on methanogenic crude oil biodegradation. *ISME J* 2(4):442–452.
6. Zengler K, Richnow HH, Rosselló-Mora R, Michaelis W, Widdel F (1999) Methane formation from long-chain alkanes by anaerobic microorganisms. *Nature* 401(6750):266–269.
7. Embree M, Nagarajan H, Movahedi N, Chitsaz H, Zengler K (2014) Single-cell genome and metatranscriptome sequencing reveal metabolic interactions of an alkane-degrading methanogenic community. *ISME J* 8(4):757–767.
8. Mee MT, Collins JJ, Church GM, Wang HH (2014) Syntrophic exchange in synthetic microbial communities. *Proc Natl Acad Sci USA* 111(20):E2149–E2156.
9. Imelfort M, et al. (2014) GroopM: An automated tool for the recovery of population genomes from related metagenomes. *PeerJ* 2:e603.
10. Overbeek R, et al. (2014) The SEED and the Rapid Annotation of microbial genomes using Subsystems Technology (RAST). *Nucleic Acids Res* 42(Database issue):D206–D214.
11. Overbeek R, et al. (2005) The subsystems approach to genome annotation and its use in the project to annotate 1000 genomes. *Nucleic Acids Res* 33(17):5691–5702.
12. Feist AM, Scholten JC, Palsson BØ, Brockman FJ, Ideker T (2006) Modeling methanogenesis with a genome-scale metabolic reconstruction of *Methanosarcina barkeri*. *Mol Syst Biol* 2:0004.
13. Yvon-Durocher G, et al. (2014) Methane fluxes show consistent temperature dependence across microbial to ecosystem scales. *Nature* 507(7493):488–491.
14. Dolfing J, Jiang B, Henstra AM, Stams AJM, Plugge CM (2008) Syntrophic growth on formate: A new microbial niche in anoxic environments. *Appl Environ Microbiol* 74(19):6126–6131.
15. Stams AJ, Plugge CM (2009) Electron transfer in syntrophic communities of anaerobic bacteria and archaea. *Nat Rev Microbiol* 7(8):568–577.
16. Lovley DR, Klug MJ (1983) Sulfate reducers can outcompete methanogens at freshwater sulfate concentrations. *Appl Environ Microbiol* 45(1):187–192.
17. Badziong W, Ditter B, Thauer R (1979) Acetate and carbon dioxide assimilation by *Desulfovibrio vulgaris* (Marburg), growing on hydrogen and sulfate as sole energy source. *Arch Microbiol* 123(3):301–305.
18. Nagarajan H, et al. (2013) Characterization and modelling of interspecies electron transfer mechanisms and microbial community dynamics of a syntrophic association. *Nat Commun* 4:2809.
19. Walker CB, et al. (2012) Functional responses of methanogenic archaea to syntrophic growth. *ISME J* 6(11):2045–2055.
20. Braun V, Patzer SI, Hantke K (2002) Ton-dependent colicins and microcins: Modular design and evolution. *Biochimie* 84(5-6):365–380.
21. Zengler K, Palsson BO (2012) A road map for the development of community systems (CoSy) biology. *Nat Rev Microbiol* 10(5):366–372.
22. Freilich S, et al. (2011) Competitive and cooperative metabolic interactions in bacterial communities. *Nat Commun* 2:589.
23. Zerbino DR, Birney E (2008) Velvet: Algorithms for de novo short read assembly using de Bruijn graphs. *Genome Res* 18(5):821–829.
24. Anders S, Huber W (2010) Differential expression analysis for sequence count data. *Genome Biol* 11(10):R106.
25. McCloskey D, et al. (2014) A model-driven quantitative metabolomics analysis of aerobic and anaerobic metabolism in *E. coli* K-12 MG1655 that is biochemically and thermodynamically consistent. *Biotechnol Bioeng* 111(4):803–815.
26. Ebrahim A, Lerman JA, Palsson BØ, Hyduke DR (2013) COBRApy: COnstraints-Based Reconstruction and Analysis for Python. *BMC Syst Biol* 7:74.
27. Hatamoto M, Imachi H, Fukayo S, Ohashi A, Harada H (2007) *Syntrophomonas palmitatica* sp. nov., an anaerobic, syntrophic, long-chain fatty-acid-oxidizing bacterium isolated from methanogenic sludge. *Int J Syst Evol Microbiol* 57(Pt 9):2137–2142.
28. Schnürer A, Zellner G, Svensson BH (1999) Mesophilic syntrophic acetate oxidation during methane formation in biogas reactors. *FEMS Microbiol Ecol* 29(3):249–261.
29. Rotaru A-E, et al. (2014) A new model for electron flow during anaerobic digestion: Direct interspecies electron transfer to *Methanosaeta* for the reduction of carbon dioxide to methane. *Energy Environ Sci* 7(1):408–415.